CHARACTERISATION OF THE ELECTRICAL RESPONSE OF A NOVEL DUAL ELEMENT THERMISTOR FOR LOW FREQUENCY APPLICATIONS

J. Schoeman and M. du Plessis

Carl and Emily Fuchs Institute for Microelectronics (CEFIM), University of Pretoria, Lynnwood Road, Pretoria, 0002, South Africa. E-mail: johan.schoeman@eng.up.ac.za

Abstract: This work is aimed at characterising the DC electrical response of a temperature sensitive microbolometer device. The contribution lies with the choice and the structure of the device, a novel bolometer infrared sensing structure consisting of dual sensing elements that are thermally very closely coupled on a single membrane supporting structure. A mathematical model is presented to characterise the behaviour of the device resistance and conductance for a given biasing current. A modified experiment of a well published non-optical method exploiting the normally unwanted Joule heating of a device when biased with a large direct current is employed for the experimental verification and validation of the theoretical model. The measured results indicate that the proposed model approximates the measured results well. Although some deviation occurs, this is to be expected and discussed.

Keywords: bolometer, electrical characterisation, MEMS, thermal microdetector, thermo isolator

1. INTRODUCTION

Bolometers are thermal microdetectors that can operate at room temperature without the need for cooling to cryogenic levels. Furthermore, they are relatively inexpensive to manufacture. It comes as no surprise that many diverse applications have been developed from this technology, including surveillance applications like night vision, enemy surveillance and border control, as well as fingerprint scanning, pollution and fire detection, spectroscopy, and medical applications like non-contact inflammation and infection detection [1–4]. It is clear that most of the current emphasis for these devices is placed in using the bolometer in the infrared (IR) range.

This work, however, is aimed at investigating and characterising the electrical response of a temperature sensitive microbolometer device (developed initially as an uncooled bolometric infrared sensing element) at much lower frequencies, enabling novel approaches to many signal processing applications. Albeit that the characterisation of the electrical properties is not new, with various DC and AC methods introduced by Shie *et al* [5–7] and others [8, 9], this characterisation is normally performed with the extraction of a signal proportional to the IR incident radiation in mind, while minimising the Joule heating caused by biasing. However, it is necessary to heat up the membrane sufficiently by applying a high power signal in order to achieve the appropriate non-linear response to demonstrate our device functionality.

The contribution of this work lies with the choice and the structure of the device. We propose a novel bolometer infrared sensing structure that consists of dual sensing elements. These elements are thermally very closely coupled on a single supporting membrane structure, as presented in Section 2. A mathematical model is derived to compensate for the new variables that are introduced in Section 3. This model is then compared to measured results from a manufactured device in Section 5, where it was found that the measured results corresponds very well with the expected theoretical behaviour proposed by the mathematical model of the device.

2. DEVICE DESCRIPTION

The device investigated in this work has a similar structure to traditional bolometer devices, but differs in that it consists of two metal resistive elements that have been layed out in such a way to ensure high thermal coupling between the two elements. The mask design of the titanium and sacrificial aluminium cantilever device prototype consisted of four mask definitions. These define the windows in the nitride layer, the lift-off mask for metal deposition, the gold pattern for interconnect and the etch of the sacrificial layer. It was decided to use a titanium metal film resistor. The fabrication has been conducted at temperatures below 500 °C to allow future post processing onto existing CMOS readout circuitry. Typical CMOS values of the material thermal parameters as reported by [10] were used for the device design. Figure 1 shows a photograph of the above device after the manufacturing process.

3. DEVICE CHARACTERISATION

It is well known that the resistance of the microbolometer

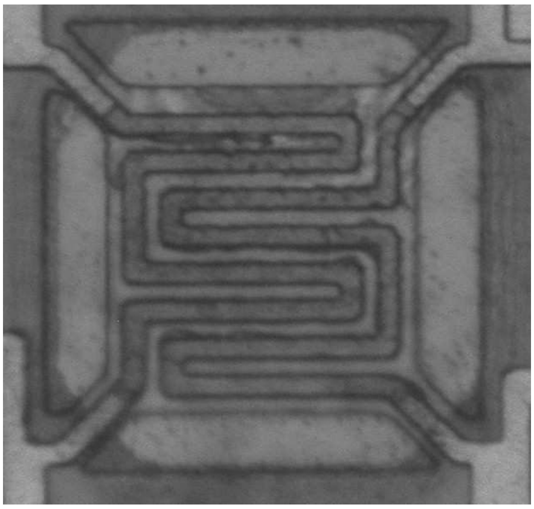

Figure 1: Photograph of the dual element bolometer device

is dependent on the difference in the active region (membrane) temperature T, or the average membrane temperature $\bar{T}$ and a chosen or reference temperature, T_0 [7]. We will assume that both the ambient temperature, T_a, and the substrate temperature, T_s, are equivalent. The microbolometer resistance of a thin-film metal device is then given as

$$R_B = R_{B0}[1 + \alpha_0(\bar{T} - T_0)] = \frac{V_B}{I_B} \quad (1)$$

with R_{B0} the reference resistance at temperature T_0 and α_0 the associated temperature coefficient of resistance (TCR). Parameter extraction of the device resistance is done by calculating the ratio of the measured voltage and current.

The next parameter of importance to device characterisation is the thermal conductance G that consists of three components, i.e. the contributions of the gaseous (G_g), radiative (G_r) and solid (G_s) conductances. We may safely assume that the radiative and solid components are neglectable, as the gaseous component contributes at least ten times more to the total conductance than the combined conductance of the radiative and solid components at atmospheric pressure. Therefore, the conductance may be given simply as [11]

$$G = G_g + G_r + G_s \approx G_g \quad (2)$$

If the thermal conductance is the dominating heat transport mechanism, it may be related to electrical parameters by means of a heat balance equation as [7, 12]

$$G(\bar{T} - T_a) = P_e + P_{IR} \quad (3)$$

where P_e is the total electrical power dissipated by the membrane and P_{IR} is the absorbed IR radiation power. The total electrical power will consist of the combined contributions of the two closely coupled resistive elements, and will be significantly larger that the contribution of the IR radiation power. Each of these resistive elements will also contribute to the change in membrane temperature, so *Eq.* (3) may be rewritten as

$$G[(\bar{T}_1 + \bar{T}_2) - T_a] = P_{e,B1} + \beta P_{e,B2} \quad (4)$$

where $\bar{T}_1$ and $\bar{T}_2$ is the average temperature rise resulting from the joule heating caused by the respective electrical power components $P_{e,B1}$ and $P_{e,B2}$. We also introduce the coupling parameter, β, that allows for inefficient coupling of electrical power due to the device structure, especially the poor coupling in the device legs, as well as the top left and bottom right corners for this topology as in Figure 1. This also compensates for the crude approximation of $\bar{T} = \bar{T}_1 + \bar{T}_2$, as these temperature components will play a more complex role than mere linear summation. The temperature rise of the membrane caused by the second resistive element is calculated as

$$\Delta T_2 = (\bar{T}_2 - T_a) = \beta P_{e,B2}/G \quad (5)$$

Notice that the additional thermal contribution of the second resistive element will also influence the temperature term of *Eq.* (1). Therefore, the resistance of the first bolometer element may be written as

$$R_{B1} = R_{B1,0}[1 + \alpha_0(\bar{T}_1 + \beta P_{e,B2}/G - T_0)] \quad (6)$$

yielding an increase in resistance of the first element equivalent to $\beta\alpha_0 R_{B1,0} P_{e,B2}/G$. This is illustrated in Figure 2 where it was assumed that $\beta = 1$. The figure also serves to further clarify the differences in the contributions of $\bar{T}_1$ and $\bar{T}_2$ respectively.

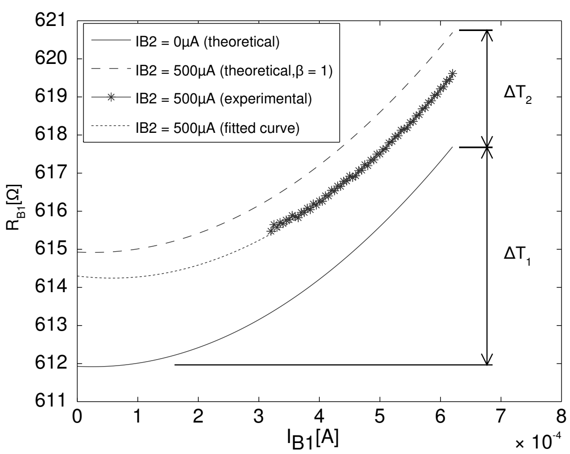

Figure 2: The effect of modulating device resistance by electric current

4. EXPERIMENTAL SETUP

Direct knowledge of α_0 is required for successful characterisation of microbolometers. This parameter is usually determined by placing the device within an oven and measuring the device voltage at a specific reference

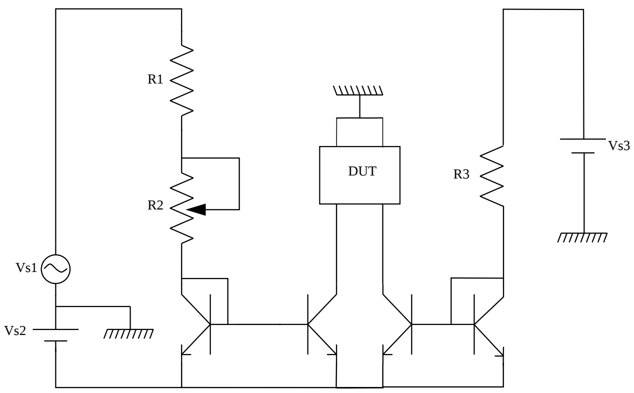

Figure 3: The implemented BJT current mirror test setup

current over a range of known temperatures [7]. From *Eq.* (2), α_0 is then determined as $\Delta R/\Delta T$. Once α_0 is known, further characterisation is possible from a DC I-V sweep, from which R_B and P_B may be determined.

Two well known methods have been published for determining the thermal conductance experimentally. The first of the two techniques require knowledge of the electrical self heating power, the device resistance and the reference parameters R_{B0} and, as mentioned earlier, α_0. R_{B0} may be determined from the I-V curve at the lowest biasing current value. Once the reference parameters have been extracted, the thermal conductance may be derived, using a simplified version of the equation presented in [7] with $T_a = T_0$, as

$$G = \frac{I_B V_B R_{B0} \alpha_0}{\frac{V_B}{I_B} - R_{B0}} \tag{7}$$

The second technique extracts the thermal conductance directly from the graph of the inverse resistance and the square of the biasing current, as discussed in [9], based on the equation

$$1/R_B = 1/R_{B0} - \alpha_0/G(I_B^2) \tag{8}$$

G may be extracted from the slope of a suitably fitted curve as $G = -\alpha/(\delta(1/R_B)/\delta(I_B^2))$.

The results of the characterisation of the first element are then used as a reference for the second part of the DC analysis. Now the second element may be stimulated by means of a controllable constant current source while the new I-V curves of the first element are measured. This has been done in incremental steps from $0\ A$ to $1\ mA$.

5. MEASURED RESULTS

The first step taken during the electrical characterisation of the device was to investigate the DC characteristics of a single element, which is then applied as a benchmark for further experimental results. All measurements were conducted with the device at atmospheric pressure. The voltage of the device was measured with a Hewlett Packard 4155B parameter analyser by applying a DC current sweep from $0\ mA$ to $1\ mA$. The resistance can then be extracted as the ratio of the measured voltage to the applied current. Note that at this stage no current was applied to the second resistive element. This result is plotted as the bottom curve labelled $R_{B0,1} = 611.9\ \Omega$ with $I_{B2} = 0\ \mu A$ in Figure 4. It is clear that the resistance is a non-linear function of current (non-ohmic), and ranges at low currents from approximately $612\ \Omega$ to $626\ \Omega$ at $1\ mA$. A numeric approach yielded a second order polynomial curve fit given as

$$R_{B0,1} = 1.63 * 10^7 I_{B1}^2 - 800 I_{B1} + 611.93 \tag{9}$$

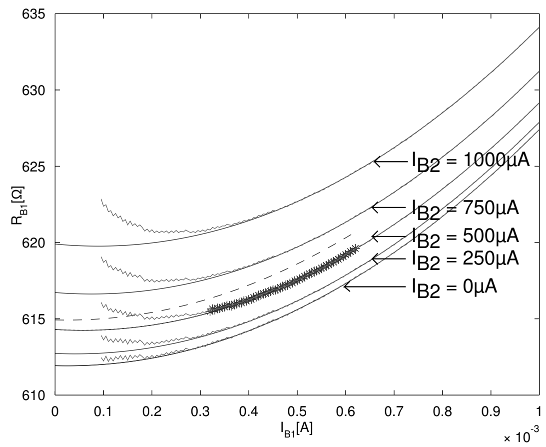

Figure 4: Device current versus resistance curve for varied I_{B2} settings

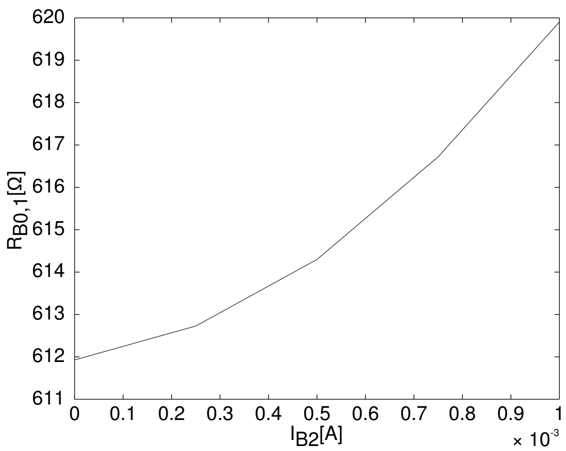

Figure 5: Effect of I_{B2} on $R_{B0,1}$

Once the benchmark result has been extracted, the DC analysis can be extended by applying various controlled DC currents to the second element, and repeating the procedure discussed earlier for every control current applied. This was done for $I_{B2} = [250, 500, 750, 1000]$

μA. The experimental results are indicated, along with the benchmark result, in Figure 4. Superimposed on this figure is theoretical graph of Figure 2, where it is applicable to note again that $P_{e,B2} = I_{B2}^2 R_{B2} = 120.1\ \mu W$ for our experimental setup at $I_{B2} = 490 \approx 500\ \mu A$. Based on *Eq.* (6) the device should experience a $\beta P_{e,B2}/G = 5.77$ degree Celcius/Kelvin increase in temperature for 100% effective coupling ($\beta = 1$), i.e. an increase of $\beta\alpha_0 R_{B1,0} P_{e,B2}/G = 2.999\ \Omega$ in device resistance. As seen from the experimental results of Figure 4 for $I_{B2} = 500\ \mu W$ that $R_{B0,1} = 614.3\ \Omega$, rather than $614.9\ \Omega$. Using this result, we find that the average membrane temperature increased only by 4.61 degree Celcius. As mentioned previously, the losses are attributed to the less than perfect coupling in the device corners. If we assume that the thermal conductance is the same in both cases, we find that approximately $93.11\ \mu W$ of the available $120.1\ \mu W$ was efficiently coupled to the first device, or $\beta = 77.5\%$. The set of curve fitted equations extracted from the experimental data is given as

$$\begin{aligned}
R_{B0,1} &= 1.63 * 10^7 I_{B1}^2 - 800 I_{B1} + 611.93 \\
R_{B0,1} &= 1.65 * 10^7 I_{B1}^2 - 1376 I_{B1} + 612.73 \\
R_{B0,1} &= 1.68 * 10^7 I_{B1}^2 - 1923 I_{B1} + 614.30 \\
R_{B0,1} &= 1.71 * 10^7 I_{B1}^2 - 2578 I_{B1} + 616.72 \\
R_{B0,1} &= 1.73 * 10^7 I_{B1}^2 - 3102 I_{B1} + 619.90
\end{aligned} \tag{10}$$

but it may also be simplified by applying *Eq.* (6) to *Eq.* (9) to relate the two resistor and current values as

$$\begin{aligned}
R_{B0,1} = \quad & 1.63 * 10^7 I_{B1}^2 - 800 I_{B1} + 611.93 \\
& +3.725 * 10^4 I_{B2}^2 R_{B2}
\end{aligned} \tag{11}$$

The effect of the control current, I_{B2}, on the resistance of the first element is plotted in Figure 5. Here we remove the effect of the device current I_{B1}.

During one of the earlier calculations we assumed that G was unaffected by the additional current, I_{B2}. One may expect that this assumption to be valid and reasonable, as the parameter is mostly dependent on material properties and surface areas which should be unaffected by biasing. However, as indicated in Figure 6 and Figure 7, it is clear that a slight increase in thermal conductance is seen as the control current is increased. This may be attributed to the fact that G is related to $\lambda_{air} A/d$, with λ_{air} the thermal conductivity of air, A the area of the device and d the distance between the membrane and the substrate. We can, therefore, conclude that a slight deformation occurs, and that the membrane to substrate distance decreases slightly due to buckling as the membrane heats up, causing the thermal conductance to increase.

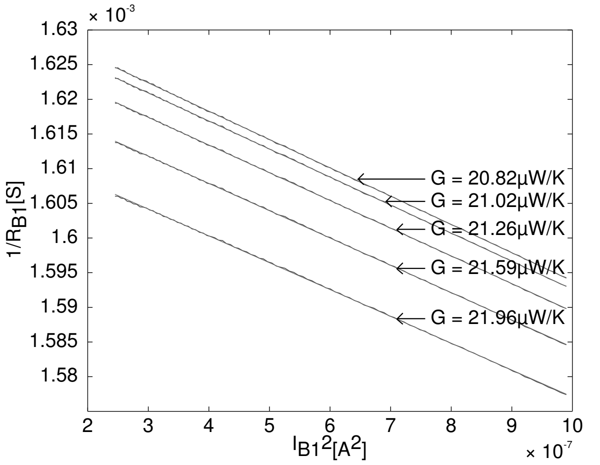

Figure 6: Thermal conductance extraction from the I_{B1}^2 vs $1/R_{B0,1}$ graph

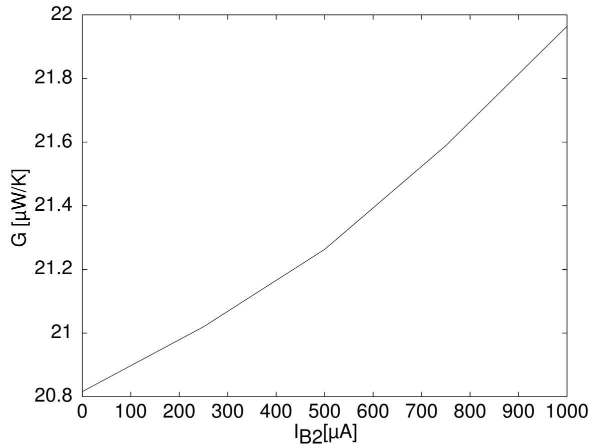

Figure 7: Effect of I_{B2} on the thermal conductance

6. CONCLUSION

A low-cost, CMOS compatible microbolometer process was previously established. Titanium was used as the sensitive resistive element, which is supported by silicon nitride. A novel device structure with a second resistive element was introducted. A mathematical model was then derived to include the effects of raising the membrane temperature by means of an electrical control signal via this second resistive element. A set of non-optical techniques have been reported for characterising and testing the manufactured uncooled microbolometer structures by increasing the Joule heating sufficiently for non-ohmic device operation. These techniques were employed to characterise the reference device parameters, before they were repeated to gauge the validity of the new device model. It was found that the introduced model behaves very similarly to the experimental results, albeit that a shaping factor, β was introduced to compensate for inefficient thermal coupling that has not been investigated analytically to date.

Previously published results indicated a very low frequency response in the low kilohertz range even at atmospheric pressure, with a preliminary indication that the MEMS device has the potential to be used in novel low frequency hybrid MEMS/CMOS IC applications where traditional CMOS failed without the use of external components. The results of this work may be applied to at least two problems found with CMOS integration. As is clear from *Eq.* (6) and Figure 2, resistance modulation is achievable by means of a control current. This allows for very fine tuning of a resistor with either an on-chip or external current source. A second problem that may be addressed is that of on-chip electrical isolation. The close coupling of the thermal energy between the resistors on the same membrane enables the transfer of an AC signal on one element to the other element, as the change in membrane temperature caused by the AC signal will result in a change in the resistance of the second element. This means that the device may be used as a micro thermal isolator, transfering an electrical signal with thermal coupling while maintaining electrical isolation between its input and output. However, the exact derivation and complete AC characterisation is reserved as a seperate investigation.

7. ACKNOWLEDGEMENTS

The authors thank the Advanced Manufacturing Technology Strategy (AMTS) of the Department of Science and Technology, South Africa for the financial support of the research.

8. REFERENCES

[1] R. Wood, “High-performance infrared thermal imaging with monolithic silicon focal planes operating at room temperature,” IEEE Electron Devices Meeting, Tech. Rep., December 1993.

[2] G. B. Jacobs and L. R. Snowman, “Laser techniques for air polution measurement,” *IEEE Journal of quantum electronics*, vol. QE-3, no. 11, pp. 603–605, November 1967.

[3] E. F. J. Ring, “The historical development of thermometry and thermal imaging in medicine,” *Journal of Medical Engineering Technology*, vol. 30, no. 4, pp. 192 – 198, July/August 2006.

[4] C. M. Travers, A. Jahanzeb, D. P. Butler, and Z. Çelik Butler, “Fabrication of semiconducting YBaCuO surface-micromachined bolometer arrays,” *Journal of Mircoelectromechanical systems*, vol. 6, no. 3, pp. 271–276, September 1997.

[5] M. Ou-Yang, C.-S. Sheen, and J.-S. Shie, “Parameter extraction of resistive thermal microsensors by AC electrical method,” *IEEE Transactions on Instrumentation and Measurement*, vol. 47, no. 2, pp. 403–408, April 1998.

[6] Y.-M. Chen, J.-S. Shie, and T. Hwang, “Parameter extraction of resistive thermal microsensors,” *Sensors and Actuators A 55*, pp. 43–47, 1996.

[7] J.-S. Shie, Y.-M. Chen, M. Ou-Yang, and B. C. S. Chou, “Characterization and modeling of metal-film microbolometer,” *Journal of Mircoelectromechanical systems*, vol. 5, no. 4, pp. 298–306, December 1996.

[8] R. Hornsey, P. Thomas, A. Savchenko, and T. Pope, “Nonoptical characterization techniques for uncooled microbolometer infrared sensors,” *IEEE Transactions on electron devices*, vol. 47, no. 12, pp. 2294–2300, December 2000.

[9] P. Eriksson, J. Y. Andersson, and G. Stemme, “Thermal characterization of surface-micromachined silicon nitride membranes for thermal infrared detectors,” *Journal of Mircoelectromechanical systems*, vol. 6, no. 1, pp. 55–61, March 1997.

[10] M. Von Arx, O. Paul, and H. Baltes, “Process-dependent thin-film thermal conductivities for thermal CMOS MEMS,” *Journal of Microelectromechanical systems*, vol. 9, no. 1, pp. 136–145, March 2000.

[11] M. Ou-Yang and J.-S. Shie, “Measurement of effective absorptance on microbolometers,” in *Instrumentation and Measurement Technology Conference, 1999. IMTC/99. Proceedings of the 16th IEEE*, vol. 1, 1999, pp. 447 –451 vol.1.

[12] F. Kohl, F. Keplinger, A. Jachimowicz, and R. Chabicovsky, “A new analytical model for detectivity prediction of resistance bolometers,” in *Sensors, 2002. Proceedings of IEEE*, vol. 2, 2002, pp. 1290 – 1293 vol.2.